ACS OMEGA

Open Access

http://pubs.acs.org/journal/acsodf

Article

Advanced Equilibrium Modeling for the Synergetic Effect of β-Cyclodextrin Integration on the Adsorption Efficiency of Methyl Parathion by β-Cyclodextrin/Exfoliated Kaolinite Nanocomposite

Nourhan Nasser, Ahmed Rady, Wail Al Zoubi,* Ahmed A. Allam, and Mostafa R. Abukhadra*

Cite This: ACS Omega 2023, 8, 48166−48180

Read Online

ACCESS | Metrics & More | Article Recommendations | Supporting Information

ABSTRACT: Exfoliated kaolinite nanosheets (EXK) and their hybridization with β-cyclodextrin (β-CD/EXK) were evaluated as potential-enhanced adsorbents of methyl parathion (MP) in synergetic investigations to determine the effects of the different modification procedures. The adsorption behaviors were described on the basis of the energetic steric and energetic factors of the specific advanced equilibrium models (monolayer model of one energy). The functionalization process with β-CD enhanced the adsorption behaviors of MP considerably to 350.6 mg/g in comparison to EXK (291.7 mg/g) and natural kaolinite (K) (244.7 mg/g). The steric studies revealed a remarkable improvement in the quantities of the existing receptors after exfoliation (N_m = 134.4 mg/g) followed by β-CD hybridization (N_m = 162.3 mg/g) as compared to K (75.7 mg/g), which was reflected in the determined adsorption capacities of MP. Additionally, each active free site of β-CD/EXK can adsorb about 3 molecules of MP, which occur in a vertical orientation by types of multimolecular mechanisms. The energetic investigations of Gaussian energy (<8.6 kJ/mol) and adsorption energy (<40 kJ/mol) validate the physical adsorption of MP, which might involve the cooperation of dipole bonding forces, van der Waals, and hydrogen bonding. The properties and entropy values, free enthalpy, and intern energy as the investigated thermodynamic functions declared the exothermic and spontaneous behaviors of the MP adsorption.

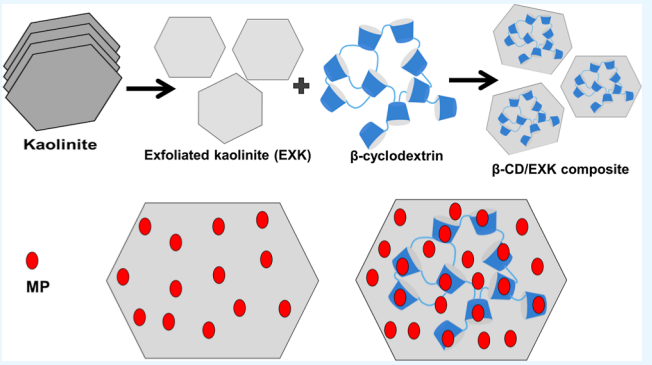

1. INTRODUCTION

In the succeeding decades, intensive industrial and agricultural operations resulted in massive volumes of discharged wastewater with substantial levels of soluble inorganic and organic contaminants.[1,2] Organic chemicals as water contaminants included pesticides, detergents, synthetic textile dyes, beauty products, medicinal residuals, pharmaceuticals, and disinfection.[3,4] Due to their extensive use in agricultural operations, a variety of pesticides have been documented as dissolved hazardous chemicals in rivers and lakes.[5,6] The majority of pesticides are classified as extremely toxic and cancer-causing contaminants, although they have an excellent effect on promoting agricultural yield.[7,8] Based on their chemical properties, pesticides are divided into inorganic chemicals, synthesized pyrethroids, organophosphates, carbamates, and organochlorines.[9]

Organophosphates are a commonly employed pesticide in agriculture owing to their great effectiveness and low cost.[9,10] Parathion (O, *O*-diethyl-*O*-4-nitro-phenyl thiophosphate), a highly effective and frequently employed organophosphorus insecticide, has been extensively determined in the world's major sources of freshwater.[11,12] The World Health Organization (WHO) designated parathion as an extremely potentially toxic and carcinogenic chemical compound that exhibits high levels of water solubility, migration and mobility, biodegradability resistance, and penetration into soil.[13,14] As a result, its presence as an organic pollutant within groundwater as well as surface water has been extensively documented, causing significant dangerous and poisonous impacts on human beings, mammals, and aquatic organisms, in addition to its hindering effect on the acetylcholinesterase enzyme within our nervous systems.[13,15]

Previous toxicity and environmental risks, as well as the deep penetration qualities of parathion insecticides into the soil's profile until groundwater, have issued significant warnings for developing appropriate remediation strategies for these types of chemicals.[15] Photocatalytic oxidation, filtration through membranes, the coagulation process, and adsorption methods are the most commonly employed techniques in the

Received: September 16, 2023
Revised: November 20, 2023
Accepted: November 23, 2023
Published: December 8, 2023

remediation of parathion insecticides.[15,16] Adsorption methods for removing such organic chemicals from water were extensively advocated in subsequent periods as simple, inexpensive, efficient, and recyclable techniques.[17,18] The cost of manufacturing, simplicity of fabricating, recycling potential, adsorption kinetics, accessibility, and adsorption capacity were considered while selecting the best materials to use as adsorbents.[12,19]

As a result, synthesized adsorbents derived from naturally occurring substances have recently been evaluated and presented as highly efficient and prospective adsorbents that might be employed for eliminating many different types of organic contaminants from water.[20,21] The purification of both organic and inorganic contaminants has been recently investigated using sophisticated modified varieties of clay mineral as cost-effective, extremely effective, and environmentally friendly structures.[22,23] Kaolinite (K) is a type of natural clay minerals that has a hydrated aluminum silicate composition and 1:1 tetrahedron/octahedron multilayered units.[24−26] Despite the fact that K is abundant naturally and relatively cost-effective as compared with other commercial clay minerals such as montmorillonite, there are insufficient studies on the mineral's potential to serve as a precursor for both environmental and medicinal uses.[22,24,27] This was attributed to the determinedly small surface area, limited ion exchange potential, and poor ability to absorb soluble ions in contrast with bentonite.[28,29] As a result, a number of modification methods, including organic hybridization, exfoliation, scrolling, polymeric integration, and inorganic surface decoration, have been effectively employed to improve both the physical and chemical characteristics of K.[29]

Exfoliation of the multilayered silicate structures of the clay minerals into separated forms of single silicate sheets with two-dimensional geometry has emerged as an advanced modification method in recent years.[22,25] This method has been employed effectively to develop unique clay nanostructures with outstanding surface reactivity, oxidization advantages, surface area, adsorption capacity, and dispersion properties.[24,30] However, whereas this technique has been widely studied for montmorillonite, very few studies have been conducted on exfoliating K and its related composites or surface-functionalized structures.[22,24] Furthermore, polymeric hybridization of the K silicate surfaces with common biopolymers produces innovative hybrid structures with substantially enhanced organophilic properties and an extensive quantity of active functional groups.[31−33]

β-Cyclodextrin (β-CD) is a frequently utilized and major oligosaccharide that has been subjected to extensive study as a vital part of different synthesized composites for a variety of environmental uses.[34,35] This was attributed mostly to its chemical stability, accessibility, adsorption characteristics, biosafety, and structural flexibility, which enabled its incorporation into a variety of composite materials.[36,37] Moreover, the β-CD form of the oligosaccharide was identified as an excellent absorbent for a wide range of soluble inorganic and organic chemicals in solutions, which could increase the quantities of the existing active sites.[38,39] However, several previously published studies demonstrate that synthetic CD-based composites as adsorbents offer an advantage over native CDs that display significant water solubility by enabling recovery and separation from the solutions, which is vital during practical and realistic applications.[39] Exfoliating K-layered units into individual layers and functionalizing them with the β-CD were expected to provide an advanced adsorbent that might be used successfully to enhance the removal of MP from water.

As a result, the research described here involved the morphological modification of K into subsequently separated and independent nanosheets (EXK) as well as their integration with β-CD polymers (β-CD/EXK) as potential adsorbents with enhanced capacities for MP toxic pesticide residuals. The adsorption experiments were carried out considering the effects of the various modification processes on the MP adsorption characteristics, including raw K, exfoliated K (EXK), and β-CD/EXK nanocomposite (β-CD/EXK) with respect to the adsorbent/adsorbate interfaces. This has been accomplished by employing experimental findings as well as theoretical parameters derived from advanced equilibrium models depending on the statistical physics theory considering both steric and energetic functions.

2. RESULTS AND DISCUSSION

2.1. Characterization of the Used Adsorbents. The XRD patterns were used to evaluate the structural changes during the formation of EXK and β-CD/EXK composites (Figure 1). The triclinic natural K mineral as a precursor was

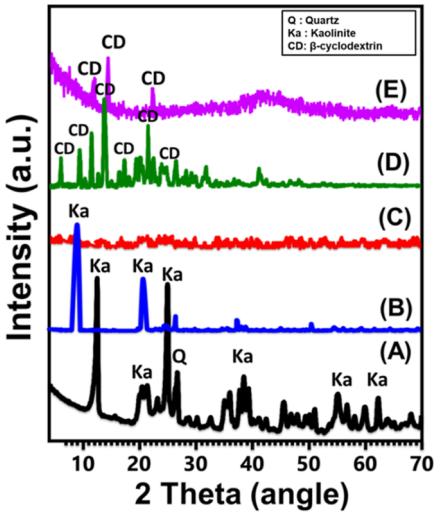

Figure 1. XRD patterns of K (A), DMSO-treated K (B), K after exfoliation (EXK) (C), β-CD polymer (D), and β-CD/EXK composite (E).

identified clearly based on its diffraction peaks [12.33° (001), 20.85° (−110), 24.87° (002), and 26.64° (111)] (Figure 1A). After the modification of K particles with DMSO, the observed pattern shows a remarkable reduction for the corresponding peaks of K, with observable detection for the main peaks only [(001) and (002)] at the deviated positions (Figure 1B). The successful exfoliation of K was confirmed by the determined XRD pattern, which characterizes the amorphous structure and complete disappearance of the corresponding crystalline peaks (Figure 1C). Comparing the obtained pattern of β-CD/EXK with the diffraction pattern of the β-CD polymer confirmed the successful hybridization of the EXK sheets with the polymer chains (Figure 1D,E). The peaks of β-CD were observed in the pattern of the β-CD/EXK composite, but with noticeable shifting and reduction in their intensities as a result of the interaction between the polymer and the chemical groups of EXK particles (Figure 1E).

https://doi.org/10.1021/acsomega.3c07088
ACS Omega 2023, 8, 48166−48180

The XRD findings are in agreement with the essential observation of the FT-IR spectra of K, EXK, and β-CD/EXK (Figure 2). The essential silicate chemical groups of K were identified clearly from the present absorption bands in its FT-IR spectrum (Si−O−Al (526 and 680 cm^{-1}), Si−O (787 and 456 cm^{-1}), Si−O−Si (1020 cm^{-1}), O−H (1641 cm^{-1}), Al−OH (912 and 3500 cm^{-1}), and Si−OH (3689 cm^{-1})) (Figure 2A).[26,41,42] The spectrum of EXK declares no significant changes in terms of the previously identified aluminosilicate chemical groups of the K units (Figure 2B). The main changes appear in the low intensities of the bands as well as their fluctuation from their original positions, in addition to the common splitting of the absorption bands at 900 and 1000 cm^{-1} (Figure 2B). This splitting is a strong indicator of the successful exfoliation of the K basic units into separated and monolayer sheets.[28,49] The spectrum of β-CD/EXK was compared to both the EXK and β-CD polymers (Figure 2C). The spectrum demonstrates the successful formation of the composite as it displays complex chemical groups related to both EXK (Si−O−Al (530 and 687 cm^{-1}), Si−O (782 and 461 cm^{-1}), Al−OH (918 and 3500 cm^{-1}), Si−O−Si (1035 cm^{-1}), and Si−OH (3690 cm^{-1})) and β-CD polymer (C═ (2932 cm^{-1}), C═C (1658.6 cm^{-1}), and C−O−C (1221 cm^{-1})) (Figure 2D).

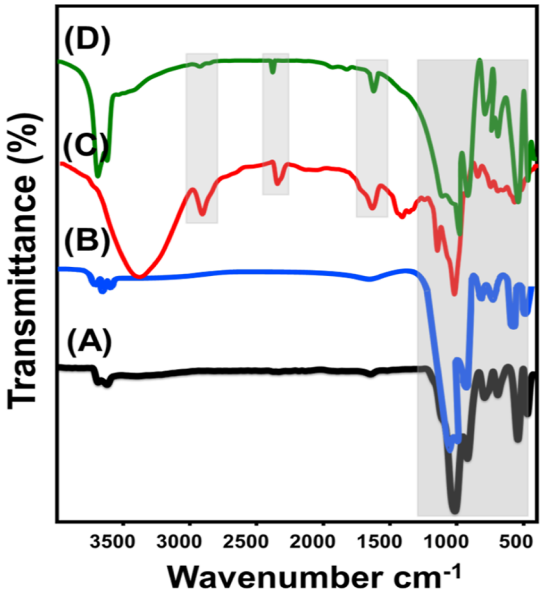

Figure 2. FT-IR spectra of K (A), K after exfoliation (EXK) (B), β-CD polymer (C), and β-CD/EXK composite (D).

The morphological impact of the different modification steps was determined based on the HRTEM images (Figure 3). Regarding the raw K, its particles are characterized as compacted pseudohexagonal flakes (Figure 3A). The HRTEM images of EXK particles reflected the significant split of the K layers, which were peeled away into monolayers (Figure 3B), which appeared with smooth outlines in some investigated images (Figure 3C). The EXK also sometimes displays observable patches, suggesting partial distortion and disordering of the basic units of K after the exfoliation modification (Figure 3D). For the HRTEM images of the β-CD/EXK composite, the detected particles display massive agglomeration properties with observable admixing between the EXK gains and the blocky polymeric matrix of the β-CD (Figure 3E,F). These morphological features are significantly in agreement with the scanning electron microscope (SEM) images that show the flakes of K impeded and functionalized with the polymer chains (Figure S1). This was reflected in the measured surface areas of the evaluated structures. The surface area increased from 10 m^2/g for K to 80.2 and 85.7 m^2/g for EXK and β-CD/EXK, respectively.

2.2. Adsorption Studies. *2.2.1. Effect of pH.* From pH 2 to pH 9, the influence of the solution's pH on the MP adsorption characteristics of K, EXK, and β-CD/EXK as efficient adsorbents has been examined. All of the aforementioned laboratory experiments were completed successfully after seriously maintaining all of the influential factors at the specified levels [MP concentration: 100 mg/L; volume: 100 mL; solid dosage: 0.2 g/L; temperature: 20 °C; and time: 120 min]. The actually determined MP uptake capacities using K, EXK, and β-CD/EXK demonstrate substantial increases corresponding to the increase in the implemented pH of the tested polluted solutions from pH 2 (1.8 mg/g (K), 5.4 mg/g (EXK), and 8.5 mg/g β-CD/EXK) toward pH 9 [57.4 mg/g (K), 102.3 mg/g (EXK), and 120.2 mg/g (β-CD/EXK)] (Figure 4). As a result, these types of structures have the ability to operate as highly efficient adsorbents during real cleaning

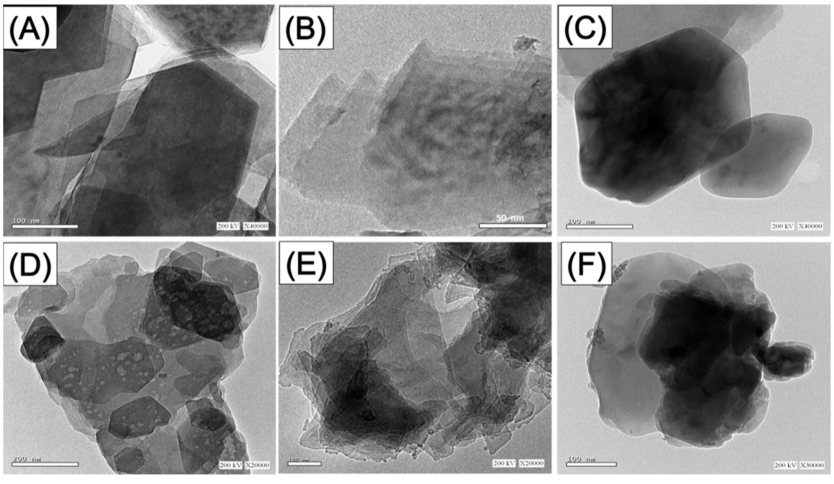

Figure 3. HRTEM image of K (A), K after exfoliation (B−D), and synthetic β-CD/EXK composite (E,F).

https://doi.org/10.1021/acsomega.3c07088
ACS Omega 2023, 8, 48166−48180

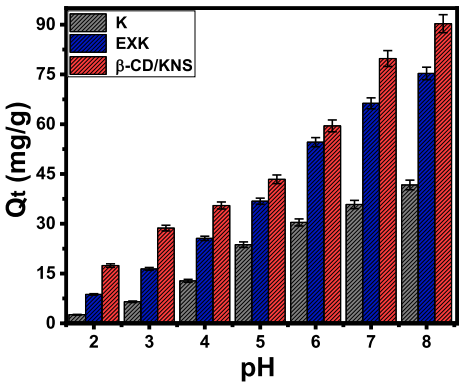

Figure 4. Influence of the pH on the uptake of MP by K, EXK, and β-CD/EXK.

operations, according to the US EPA's recommended pH range for industrial wastewater (pH 6 to 9).[43] The observed behaviors are strongly correlated with the significant influence of pH on the MP ionization behaviors and the dominating charges on the outside surfaces of K, EXK, and β-CD/EXK.[44] The chemically active groups of K, EXK, and β-CD/EXK were continuing to deprotonate as the alkaline levels of MP solutions escalated, and their outermost layers became totally saturated with negative electrical charges.[45] Since the exteriors of K, EXK, and β-CD/EXK are dominated by negative charges, they act as centers for the electrostatic attractions for the positively charged soluble molecules of MP.[21] The established pH values of these structures are in agreement with the previously reported uptake behaviors of MP as a function of solution pH [$pH_{(ZPC)}$ = 7 (K), 7.3 (EXK), and 6.4 (β-CD/EXK)].

2.2.2. Effect of Contact Time. The experimental influence of the MP uptake duration on the actually determined capacities of K, EXK, and β-CD/EXK has been examined over a studied time range of 30−840 min. This was accomplished after fixing the other affecting factors at certain values [MP concentration: 100 mg/L; pH: 9; volume: 100 mL; temperature: 20 °C; and solid dosage: 0.2 g/L]. The uptake behaviors K, EXK, and β-CD/EXK as efficient adsorbents of MP exhibit remarkable increases in terms of the detectable uptake rates as well as the measured adsorbed MP quantities in MP/g, together with the controlling rise of the duration of the tests (Figure 5A). This observable enhancement effect of the MP uptake behaviors using K, EXK, and β-CD/EXK can be identified clearly up to 240 min. Following this contact interval, neither the MP uptake rates nor the quantities of adsorbed MP exhibited any noticeable changes or increments, indicating states of stability known as adsorption equilibrium states (Figure 5A). Throughout these stages, the MP equilibrium absorption capacities of the K, EXK, and β-CD/EXK particulates are 83.8 mg/g (K), 147.2 mg/g (EXK), and 186.2 mg/g (β-CD/EXK) (Figure 5A). The observable high MP uptake rates and the rapid rises in the MP adsorbed quantities have been triggered by the existence of numerous free and reactive functional groups or uptake receptors on the surfaces of K, EXK, and β-CD/EXK during the starting duration of the experiments.[20] Prolonged MP absorption into the receptors of K, EXK, and β-CD/EXK results in their

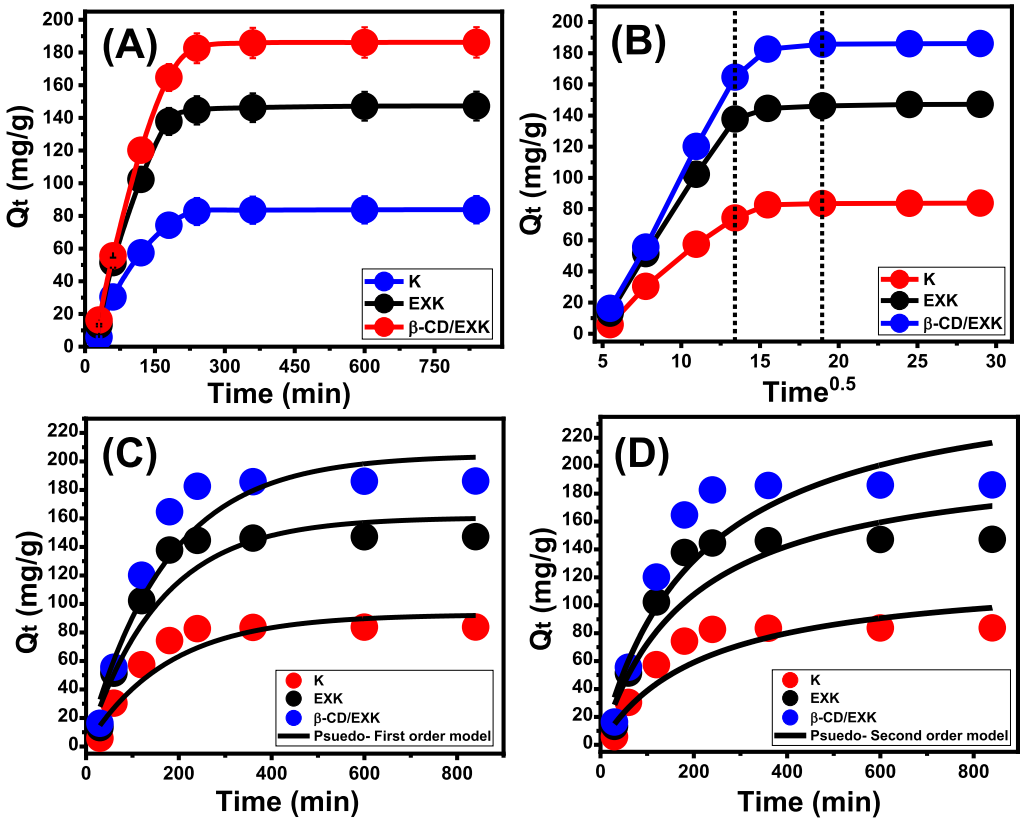

Figure 5. Effect of the contact time on the uptake of MP by K, EXK, and β-CD/EXK (A), the intraparticle diffusion curves of the MP uptake results by K, EXK, and β-CD/EXK (B), fitting of the MP adsorption results with the pseudo-first-order kinetic model (C), and fitting of the MP adsorption results with the pseudo-second-order kinetic model (D).

https://doi.org/10.1021/acsomega.3c07088
ACS Omega 2023, 8, 48166−48180

occupancy and consumption, which sharply reduces their availability as the period of the experiments is increased. As a result, following a specific time duration, the MP experimental uptake rates drastically declined, and K, EXK, and β-CD/EXK exhibit ignored or no changes in their uptake characteristics. After the MP had fully filled all of the receptors or the present reactive sites, the equilibrium states of K, EXK, and β-CD/EXK were identified.[2]

2.2.3. Intraparticle Diffusion Behavior. Intraparticle diffusion curves for the MP uptake activities by K, EXK, and β-CD/EXK establish three distinct segments that have various slopes (Figure 5B). These obtained curves also show no discernible crossings with the original points, demonstrating the cooperation of more than one adsorption mechanism alongside the effect of MP diffusion processes.[44,46] The operating mechanism might include (A) the adsorption of MP by the distributed receptors on the outer surfaces of K, EXK, and β-CD/EXK (border), (B) intraparticle diffusion, and (C) the operating reaction of the saturation and equilibrium stages.[47] The first stage demonstrates that the external MP adsorption processes were the most effective mechanisms by initiating the tests, and the efficiency of the MP uptake reaction in this stage relies on the overall amounts of surficial active receptors of K, EXK, and β-CD/EXK (Figure 5B).[48] By prolonging the period, new stages were detected, which indicates the effectiveness of different extra mechanisms known as layered adsorption processes (Figure 5B).[12,48] These other mechanisms also involve the influence of MP diffusion activities. Finally, it has been observed that the third and last stages are predominant if K, EXK, and β-CD/EXK are in their equilibrium states of MP adsorption. This demonstrates that the sequestered MP molecules have fully filled or consumed all the existing effective binding sites (Figure 5B).[19,44] At this stage, MP adsorption is controlled by a number of processes, some of which may involve molecular interactions and/or interionic attraction mechanisms.[45]

2.2.4. Kinetic Modeling. The kinetic properties of the MP uptake operations via K, EXK, and β-CD/EXK have been illustrated using the conventional kinetic assumptions of the pseudo-first-order (P.F.) as well as pseudo-second-order (P.S.) models. The level of agreement between the MP uptake behaviors and the kinetic suggestions of the two models was assessed based on the determined nonlinear fitting criteria with their representative formulas according to both correlation coefficient (R^2) and Chi-squared (χ^2) (Table 1 and Figure 5C,D). The obtained values of R^2 coupled with χ^2 revealed a better fit of MP adsorption behaviors via K, EXK, and β-CD/EXK with the kinetic functions and principles of the P.F. model than those of the assessed P.S. model. The remarkable agreement that existed between the experimentally established capacities of K, EXK, and β-CD/EXK at their equilibrium states [83.8 (K), 147.2 (EXK), and 186.2 mg/g (β-CD/EXK)] and the mathematically derived values [92.6 (K), 160.7 (EXK), and 204.4 mg/g (β-CD/EXK)] confirmed previous kinetic findings (Table 1). According to the kinetic basics of the P.F. model, physical mechanisms, such as van der Waals forces and/or electrostatic attraction, may have played the dominant influence during the sequences of MP by K, EXK, and β-CD/EXK.[49,50] Even though the P.F. model's formula for eliminating MP by K, EXK, and β-CD/EXK is more matched than the P.S. model's depicted formula, the uptake behaviors nevertheless exhibit considerable agreement with the P.S. kinetics. Therefore, it was predicted that a number of frequently occurring weak chemical processes, such as chemical complexing, hydrogen binding, hydrophobic interaction, and electron sharing, would either have a supportive role or have minimal impact on the uptake of MP by K, EXK, and β-CD/EXK.[44,49] A physical uptake the MP layer was developed after a chemically adsorbed MP layer using the first one as the substrate.[51]

Table 1. Mathematical Parameters of the Studied Kinetic Models

material	model	parameters	values
K	pseudo-first-order	K_1 (1/min)	0.0057
		$Q_{e(Cal)}$ (mg/g)	92.65
		R^2	0.91
		X^2	3.7
	pseudo-second-order	k_2 (mg/g min)	3.6×10^{-5}
		$Q_{e(Cal)}$ (mg/g)	123.94
		R^2	0.89
		X^2	5.01
EXK	pseudo-first-order	K_1 (1/min)	0.0063
		$Q_{e(Cal)}$ (mg/g)	160.69
		R^2	0.93
		X^2	4.85
	pseudo-second-order	k_2 (mg/g min)	2.5×10^{-5}
		$Q_{e(Cal)}$ (mg/g)	209.84
		R^2	0.90
		X^2	7.04
β-CD/EXK	pseudo-first-order	K_1 (1/min)	0.0058
		$Q_{e(Cal)}$ (mg/g)	204.44
		R^2	0.94
		X^2	5.4
	pseudo-second-order	k_2 (mg/g min)	1.7×10^{-5}
		$Q_{e(Cal)}$ (mg/g)	270.49
		R^2	0.91
		X^2	8.005

2.2.5. Effect of MP Concentrations. Within the experimentally evaluated range of 100−700 mg/L, the influence of the starting MP concentrations was assessed to determine the actual optimum capacities of K, EXK, and β-CD/EXK in addition to their equilibrium properties. The other uptake factors were selected at specified values [solid dosage: 0.2 g/L; time: 24 h; volume: 100 mL; and temperature: 298, 308, and 313 K]. The experimental quantities of MP adsorbed by K, EXK, and β-CD/EXK increased significantly at the higher levels of MP starting concentrations (Figure 6A−C). The elevated concentrations of MP ions within a given volume caused a noticeable increase in their mobility, diffusion, and driving forces, which improved their interactions and collision chances with the majority of the existing free and active receptors found on the exterior surfaces of K, EXK, and β-CD/EXK. As a result, the effectiveness of the MP adsorption processes by K, EXK, and β-CD/EXK was greatly enhanced.[31] The increase in the adsorbed quantities of MP in terms of the adjusted starting concentration can be noticed up to the specified examined values. Afterward, an increase in the beginning MP concentrations has an ignored detrimental impact on the quantities of its adsorbed molecules by K, EXK, and β-CD/EXK, which distinguishes their equilibrium states and attends to the actual maximal MP uptake capacities.

The equilibrium states in the existence of K that can be recognized after 600 mg/L are associated with adsorption capacities of 232.1 mg/g (298 K), 209.3 mg/g (308 K), and

https://doi.org/10.1021/acsomega.3c07088
ACS Omega 2023, 8, 48166−48180

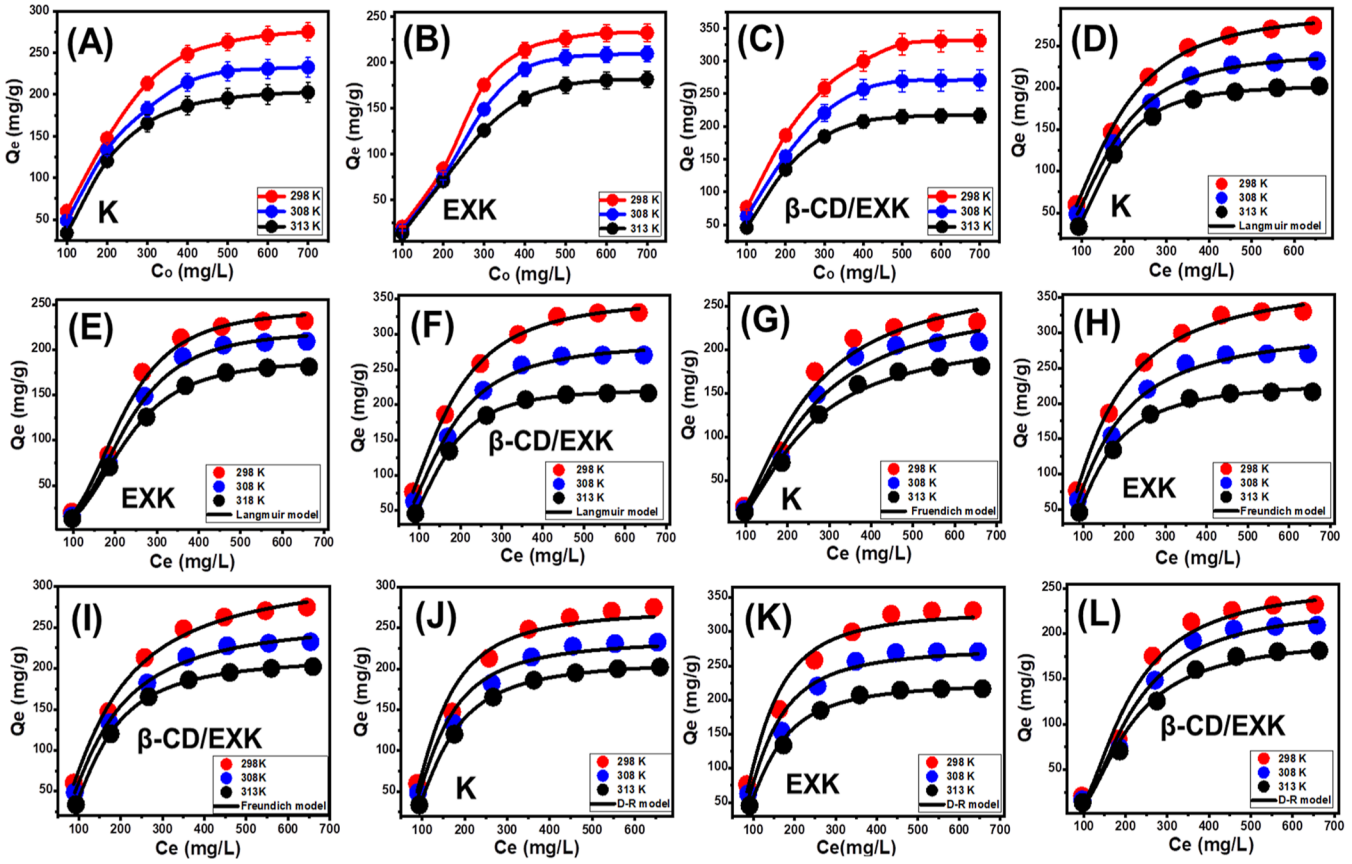

Figure 6. Shows the impact of the starting MP concentrations on the uptake capacities of the studied adsorbents [(A) (K), (B) (EXK), and (C) (*β*-CD/EXK)], fitting of the MP adsorption results with classic Langmuir model [(D) (K), (E) (EXK), and (F) (*β*-CD/EXK)], fitting of the MP uptake results with classic Freundlich model [(G) (K), (H) (EXK), and (I) (*β*-CD/EXK)], and fitting of the MP adsorption results with classic D-R model [(J) (K), (K) (EXK), and (L) (*β*-CD/EXK)].

181.4 mg/g (313 K) (Figure 6A). For EXK, the detected equilibrium capacities are 275.1 mg/g (298 K), 232.6 mg/g (308 K), and 202.4 mg/g (313 K) (Figure 6B). For *β*-CD/EXK, the equilibrium concentration is 500 mg/L and the corresponding equilibrium adsorption capacities are 330.8 mg/g (298 K), 270.6 mg/g (308 K), and 216.5 mg/g (313 K) (Figure 6C). The notable high uptake abilities of *β*-CD/EXK during the elimination of MP in versus K and EXK free particles could be attributed to (1) the increased surface area, (2) the substantial rise in the overall number of active sites after the incorporation of the *β*-CD chains, and (3) the significant improvement in the composite's organophilicity when compared to hydrophilic K and EXK. The observed decrease in the adsorption of MP by K, EXK, and *β*-CD/EXK in relation to the test temperature indicated that the reactions were exothermic.

2.2.6. Giles's Classification. The categorization of the MP isotherm curves utilizing K, EXK, and *β*-CD/EXK based on the ascribed criteria of Giles' classification revealed that they formed L-type equilibrium curves (Figure 6A−C). The L-type equilibrium characteristics contribute to the significant and powerful impacts caused by intermolecular attraction forces throughout the adsorption processes of MP by the K, EXK, and *β*-CD/EXK particles, together with the substantial interaction between the MP molecules and the highly reactive chemical structures of K, EXK, and *β*-CD/EXK.[52] A full production of adsorbed MP monolayers on the outermost surfaces of K, EXK, and *β*-CD/EXK particles was also potentially predicted based on L-type isotherm characteristics.[26] Furthermore, this isothermal behavior suggests the formation of K, EXK, and *β*-CD/EXK particles with numerous types of both active and free uptake receptors that exhibit substantial selectivity to the MP molecules throughout their adsorption, particularly at low starting concentrations.

2.2.7. Classic Isotherm Models. The equilibrium suggestions of the MP uptake behaviors by the K, EXK, and *β*-CD/EXK particulates have been investigated according to the isotherm concepts of the traditional Langmuir-, Freundlich-, and Dubinin-Radushkevich (D-R) models. The concordance between the equilibrium suggestions in every one of the mentioned models and experimentally detected MP uptake activities was evaluated depending on the marked nonlinear fit levels with the relevant formulas of the individual models, considering the R^2 together with χ^2 (Table 2 and Figure 6D−L). The values of R^2 and χ^2 demonstrated a more favorable fit of the MP uptake behaviors by K, EXK, and *β*-CD/EXK particulates with the Langmuir isotherm's concepts than with the fundamental properties of the Freundlich assumptions (Table 2 and Figure 6D−L). The Langmuir isotherm donates the adsorption of MP homogeneously throughout the unfilled and active uptake receptors of K, EXK, and *β*-CD/EXK particulates in monolayer arrangements.[49,50] Additionally, the MP uptake performances by K, EXK, and *β*-CD/EXK particulates have estimated RL values that are lower than 1, showing that the reactions possess favorable properties.[20,48] The expected maximal MP absorption capacities (Q_{max}) of K

https://doi.org/10.1021/acsomega.3c07088
ACS Omega 2023, 8, 48166−48180

Table 2. Mathematical Parameters of the Studied Classic Isotherm Models

			298 K	308 K	313 K
K	Langmuir model	Q_{max} (mg/g)	244.79	221.56	189.15
		b (L/mg)	3.03×10^{-8}	2.7×10^{-8}	3.9×10^{-8}
		R^2	0.995	0.997	0.999
		X^2	0.69	0.33	0.02
	Freundlich model	$1/n$	0.57	0.58	0.57
		k_F (mg/g)	283.76	258.92	217.65
		R^2	0.98	0.99	0.996
		X^2	1.97	1.38	0.574
	D-R model	β (mol^2/KJ^2)	0.011	0.012	0.0116
		Q_m (mg/g)	254.17	230.37	194.43
		R^2	0.98	0.983	0.99
		X^2	2.38	1.86	0.87
		E (kJ/mol)	6.74	6.45	6.56
EXK	Langmuir model	Q_{max} (mg/g)	292.25	243.2	203.29
		b (L/mg)	1.5×10^{-5}	5.2×10^{-6}	2.2×10^{-7}
		R^2	0.997	0.998	0.999
		X^2	0.056	0.049	0.038
	Freundlich model	$1/n$	0.67	0.59	0.48
		k_F (mg/g)	313.74	259.76	213.45
		R^2	0.99	0.99	0.99
		X^2	0.43	0.513	0.185
	D-R model	β (mol^2/KJ^2)	0.0081	0.0083	0.0092
		Q_m (mg/g)	272.3	235.18	209.59
		R^2	0.97	0.98	0.99
		X^2	1.55	0.67	0.037
		E (kJ/mol)	7.85	7.76	7.37
β-CD/EXK	Langmuir model	Q_{max} (mg/g)	351.97	287.5	222.2
		b (L/mg)	1.8×10^{-5}	9.3×10^{-6}	8.9×10^{-7}
		R^2	0.999	0.998	0.999
		X^2	0.064	0.16	0.017
	Freundlich model	$1/n$	0.66	0.61	0.5
		k_F (mg/g)	378.7	308.8	231.6
		R^2	0.998	0.995	0.998
		X^2	0.29	0.47	0.31
	D-R model	β (mol^2/KJ^2)	0.0067	0.0081	0.0086
		Q_m (mg/g)	330.35	275.24	225.26
		R^2	0.98	0.982	0.99
		X^2	1.53	1.18	0.16
		E (kJ/mol)	8.63	7.85	7.62

are 244.7 (298 K), 221.5 (308 K), and 189.1 mg/g (313 K), and the computed values using EXK are 292.2 (298 K), 243.2 (308 K), and 203.3 mg/g (313 K). For β-CD/EXK, the theoretical Q_{max} values are 351.9 mg/g (298 K), 287.6 mg/g (303 K), and 222.2 mg/g (313 K) (Table 2).

The D-R model's isotherm theories (Figure 6J–L) clarify the energetic changes of K, EXK, and β-CD/EXK particulates during the sequestration of the MP, regardless of heterogeneity or homogeneity.[53] The Gaussian energy (E) as a mathematical parameter from the D-R assessment approach is a key to determining which types of MP uptake mechanisms (chemical or physical) impact the adsorption processes. Adsorption activities with E values of <8, 8–16, and >16 kJ/mol, respectively, are indicative of the involvement of highly physical, weak chemical, and/or complex physical/chemical and influential chemical processes.[20,53] The values that have been determined for the E factor of MP uptake behaviors by K, EXK, and β-CD/EXK fall within the assumed energy levels that were suggested for the physical procedures (<8 kJ/mol) in agreement with the theoretical findings of the kinetic studies (Table 2). The E values for the uptake of MP by the β-CD/EXK composite match the suggested limits of physical processes and roughly the specified range of complex physical/chemical mechanisms or poor chemical processes as well.

2.2.8. Advanced Isotherm Modeling. According to the assumptions of statistical physics theory, the most recently assessed advanced equilibrium models could greatly reveal the distinctive features of the adsorption reactions with respect to the adsorbent/adsorbate interfaces and the exterior aspects of the mixed solid adsorbents. The fitting mathematical components developed using such models, such as the energetic and steric variables, may be employed to illustrate the mechanistic steps. The steric variables comprised the overall number of MP molecules occupied in each site ($n_{(MP)}$), the quantities of consumed sites by the MP on the surfaces of K, EXK, and β-CD/EXK ($N_{m\ (MP)}$), and the uptake capacity of K, EXK, and β-CD/EXK under the state of saturation ($Q_{sat\ (MP)}$). The energetic components were the internal energy (E_{int}), free enthalpy (G), entropy (S_a), and MP absorption

https://doi.org/10.1021/acsomega.3c07088
ACS Omega 2023, 8, 48166−48180

energy (E). A mathematical model of MP uptake activities has been carried out based on nonlinear fits using the corresponding equations of these models. This was done via the use of multivariable nonlinear regression modeling and the Levenberg−Marquardt iterative approach. On the basis of the revealed fitting degrees, a monolayer model with one energy site was implemented to characterize the MP adsorption processes by K, EXK, and β-CD/EXK (Table 3 and Figure 7A−C).

Table 3. Mathematical Parameters of the Studied Advanced Isotherm Model

advanced isotherm model				
steric and energetic parameters				
		298 K	308 K	313 K
K	R^2	0.995	0.997	0.999
	X^2	0.69	0.33	0.021
	n	3.229	3.227	3.163
	N_m (mg/g)	75.78	68.64	59.78
	Q_{Sat} (mg/g)	244.69	221.5	189.08
	$C_{1/2}$ (mg/L)	222.61	220.65	218.96
	ΔE (kJ/mol)	−9.39	−8.49	−8.03
EXK	R^2	0.993	0.994	0.995
	X^2	0.0568	0.0492	0.038
	n	2.17	2.39	3.02
	N_m (mg/g)	134.46	101.5	67.31
	Q_{Sat} (mg/g)	291.77	242.52	203.27
	$C_{1/2}$ (mg/L)	165.56	160.78	158.34
	ΔE (kJ/mol)	−8.67	−7.68	−7.18
β-CD/EXK	R^2	0.999	0.998	0.997
	X^2	0.064	0.16	0.017
	n	2.16	2.29	2.78
	N_m (mg/g)	162.35	125.11	79.73
	Q_{Sat} (mg/g)	350.67	286.5	221.64
	$C_{1/2}$ (mg/L)	156.58	154.11	148.04
	ΔE (kJ/mol)	−8.53	−7.57	−7.01

2.2.8.1. Steric Properties. Number of adsorbed MP ($n_{(MP)}$) per each site: The numerical results of the $n_{(MP)}$ factor greatly imply the orientation (vertical or horizontal) of the pesticide molecules that were adsorbed on the exteriors of K, EXK, and β-CD/EXK, in addition to their significance about the controlling mechanistic activities (multi-docking versus multi-interactions). One MP molecule is sequestered by several adsorption sites in horizontal arrangements in those processes, which are most influenced by multi-anchorage or multi-docking mechanisms. Processes that display values beyond 1, 2, or more MP molecules can be captured by only one active site in nonparallel and vertical orientations, and these uptake activities are mainly mediated by multi-ionic mechanistic operations.[20,54] The observed $n_{(MP)}$ values for K ($n_{(MP)}$ = 3.16−3.22), EXK ($n_{(MP)}$ = 2.17−3.2), and β-CD/EXK ($n_{(MP)}$ = 2.16−2.78) are more than 1 (Figure 7D−F and Table 3). As a result, the MP molecules were taken up via multimolecular mechanistic processes, whereby each uptake site of the adsorbents could receive up to 4 ions (K and EXK) and 3 molecules (β-CD/EXK), which were oriented vertically in nonparallel properties.

In terms of temperature effects, the computed $n_{(MP)}$ values of K demonstrate detectable declination as the tested temperature increases from 298 to 313 K (Figure 7D−F). This was ascribed to the expected decrease in MP aggregation properties during its uptake on the K structure under high temperature conditions.[31] This behavior was reversed during the uptake processes by both EXK and β-CD/EXK as the values increased considerably after a regular increase in the temperature. This suggested a significant impact of the exfoliation and polymeric hybridization processes on the surface properties and reactivity of the obtained products. This might result in a notable increase in the aggregation affinities of MP molecules on the surfaces of EXK and β-CD/EXK. This further demonstrates the existence of thermal (energetic) activating processes before MP is captured on the exterior of K.[17,55]

Occupied active sites density (N_m): The density of the MP-occupied sites ($N_{m\ (MP)}$) of K, EXK, and β-CD/EXK substantially represents the total quantity of the free and efficient adsorption receptors across the exteriors of its nanoparticles during the reaction (Figure 7G−I and Table 3). The computed $N_{m\ (MP)}$ values for K are 75.78 mg/g (298 K), 68.64 mg/g (308 K), and 59.78 mg/g (313 K) (Figure 7G). These values enhanced greatly after the exfoliation modifications (EXK) to be 134.46 mg/g (298 K), 101.5 mg/g (308 K), and 67.31 mg/g (313 K) (Figure 7H). Furthermore, the existence of the active sites was greatly enhanced after the integration of the β-CD polymer (β-CD/EXK) to be 162.35 mg/g (298 K), 125.11 mg/g (308 K), and 79.73 mg/g (313 K) (Figure 7I and Table 3). These findings confirm a significant increase in the total number of existing reactive sites after the exfoliation modification of K, forming single nanosheets, and the combination of EKX and β-CD polymers, producing the β-CD/EXK composite. This has been attributed primarily to the corresponding increase in surface area, exposure of the siloxane active chemical groups, and the insertion of extra active functional sites following the development of the composite, all of which induced an interactive interface that existed between the MP solutions and the surfaces of the EXK and β-CD/EXK composite. Regarding the effects of temperature, the $N_{m\ (MP)}$ values of EXK and β-CD/EXK exhibit reversible correlations with temperature (Figure 7G−I and Table 3). This is compatible with earlier reported $n_{(MP)}$ values since an increase in aggregation affinities of MP reduces the overall number of filled adsorption sites, together with the influence of temperature on the dominating status of the existing active sites.[17,56]

Adsorption capacity at the saturation state of (Q_{sat}): The maximum uptake capacities are best predicted by the MP adsorption characteristics of K, EXK, and β-CD/EXK in their saturation (Q_{sat}) status. The realized density of the occupied sites (N_m) and the overall quantity of MP molecules attracted by each site (n) have a significant effect on the results of Q_{sat}. As a potential adsorbent of MP, K has computed Q_{sat} values of 244.69 (298 K), 221.5 (308 K), and 189.08 mg/g (313 K) (Figure 7J and Table 3). Regarding the exfoliated product (EXK), it has potential enhanced uptake capacities up to 291.7 mg/g (298 K), 242.5 mg/g (308 K), and 203.3 mg/g (313 K) (Figure 7K and Table 3). This enhancement increased significantly after the hybridization of EXK with β-CD to be 350.6 mg/g (298 K), 286.5 mg/g (308 K), and 221.6 mg/g (313 K) (Figure 7L and Table 3). The exothermic characteristics of MP uptake activities by K, EXK, and β-CD/EXK have been concluded from the temperature's adverse effects (Figure 6I−L and Table 4). Additionally, this demonstrated the accelerating impact of the uptake temperature on the thermal collision properties of the reaction system, which results in a reduction in the efficiency of MP adsorption.[54] Additionally,

https://doi.org/10.1021/acsomega.3c07088
ACS Omega 2023, 8, 48166−48180

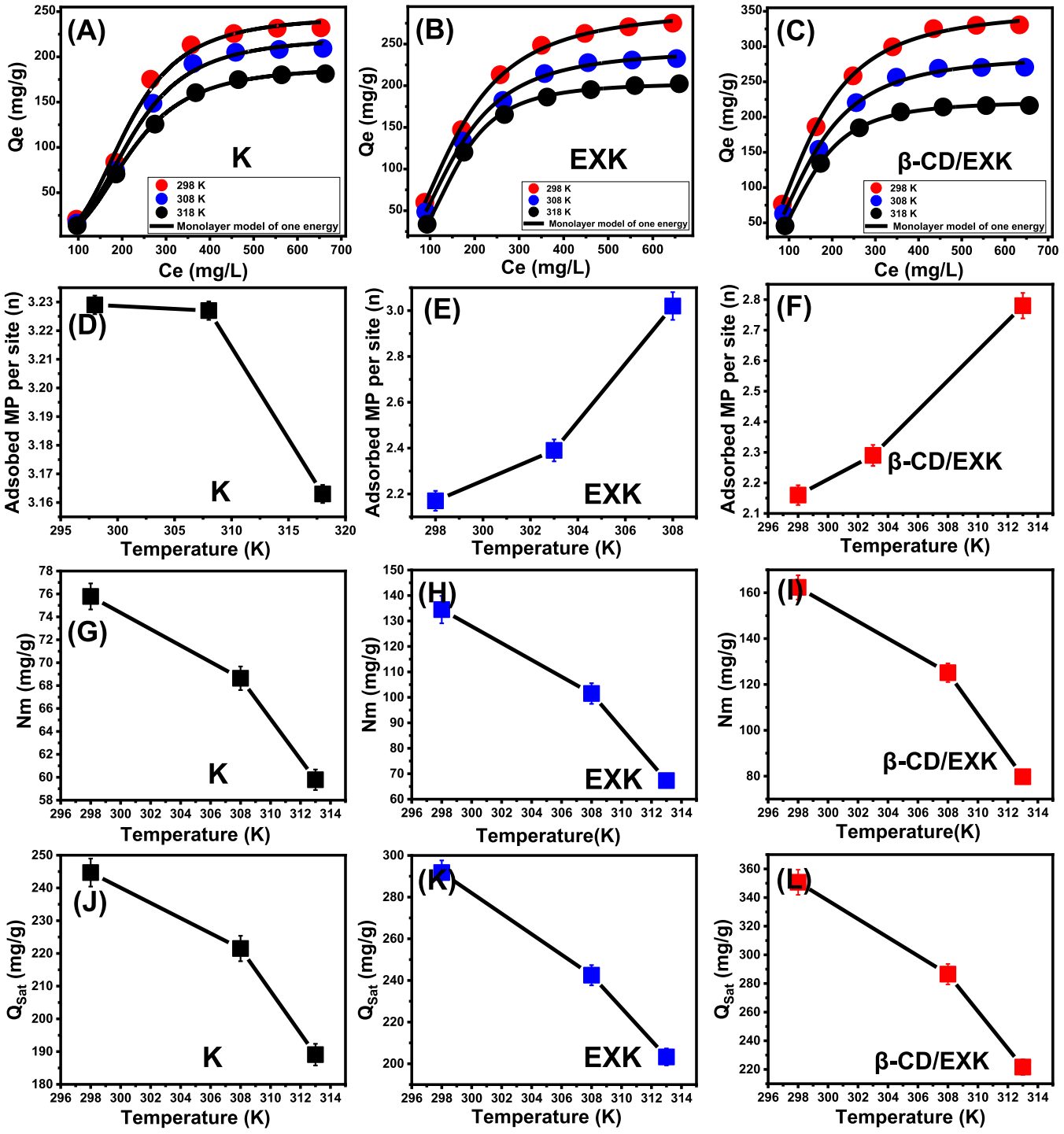

Figure 7. Shows fitting of the MP adsorption results of MP with an advanced monolayer model of one energy [(A) (K), (B) (EXK), and (C) (*β*-CD/EXK)], changes in the number of adsorbed MP molecules per each active site [(D) (K), (E) (EXK), and (F) (*β*-CD/EXK)], changes in the active site density during the uptakes of MP [(G) (K), (H) (EXK), and (I) (*β*-CD/EXK)], and changes in the dyes adsorption capacities during the saturation states [(J) (K), (K) (EXK), and (L) (*β*-CD/EXK)].

the resulting Q_{sat} qualities as a result of uptake temperature show remarkable agreement with the earlier reported behaviors of N_m as in contrast to those of n, implying that the active sites are the essential and control regulators of the effectiveness of MP adsorption rather than the potential capacity of each active site.

2.2.8.2. Energetic Properties. Adsorption energy: The energies (ΔE) of MP uptake processes may reliably suggest the type that regulates mechanisms, either chemical or physical. Chemical mechanisms have energies more than 80 kJ/mol, whereas physical reactions have energies less than 40 kJ/mol. The physically occurring mechanistic activities are further divided into many different categories based on the adsorption energy levels. These involve hydrogen binding (<30 kJ/mol), the attraction of van der Waals (4−10 kJ/mol), dipole binding forces (2−29 kJ/mol), coordinating exchange (40 kJ/mol), and hydrophobic binding (5 kJ/mol).[31,57] The measured values of the MP uptake energies (E) have been

https://doi.org/10.1021/acsomega.3c07088
ACS Omega 2023, 8, 48166−48180

Table 4. Comparison between the Addressed β-CD/EXK as Adsorbent and Other Evaluated Materials in Literature

adsorbents	Q_{max} (mg/g)	references
MP		
activated carbon	104.9	60
zeolite-A	83.4	61
Senegal River Typha Australis	7.67	62
βeta-CD	42.3	61
clay soil	12.4	63
CD/ZA composite	368.7	61
chitosan	23.2	64
red soil	8.6	63
cellulose	77.9	64
Fe^0-CH/CF	237.8	64
K	**244.69**	**this study**
EXK	**291.77**	**this study**
β-CD/EXK	**350.67**	**this study**

determined mathematically via eq 1 utilizing the measured solubility of MP in the water solution (S), gas constant (R = 0.008314 kJ/mol·K), MP concentrations during the half saturation states of K, EXK, and β-CD/EXK, and absolute temperature (T)[58]

$$\Delta E = RT \ln\left(\frac{S}{C}\right) \quad (1)$$

The energies estimated for MP sequestration by K and EXK are within the range of −9.39 to −8.03 and −9.38 to −16.49 kJ/mol, respectively (Table 3), while the estimated values for β-CD/EXK varied from −8.53 to −7.01 kJ/mol (Table 4). Therefore, the absorption of MP by K, EXK, and β-CD/EXK was mainly mediated by physical processes that include the forces of dipole binding forces (2 to 29 kJ/mol), van der Waals (4 to 10 kJ/mol), and hydrogen bonding (30 kJ/mol). Furthermore, the negative signs of the computed values of E for the capturing of MP by K, EXK, and β-CD/EXK correlate with the results of the tests regarding the exothermic properties of the occurring process.

Entropy: The entropy (S_a) of the MP uptake behaviors by K, EXK, and β-CD/EXK readily reveals the order and disorder characteristics of the surfaces of their particles under the impact of different evaluated concentrations of MP in addition

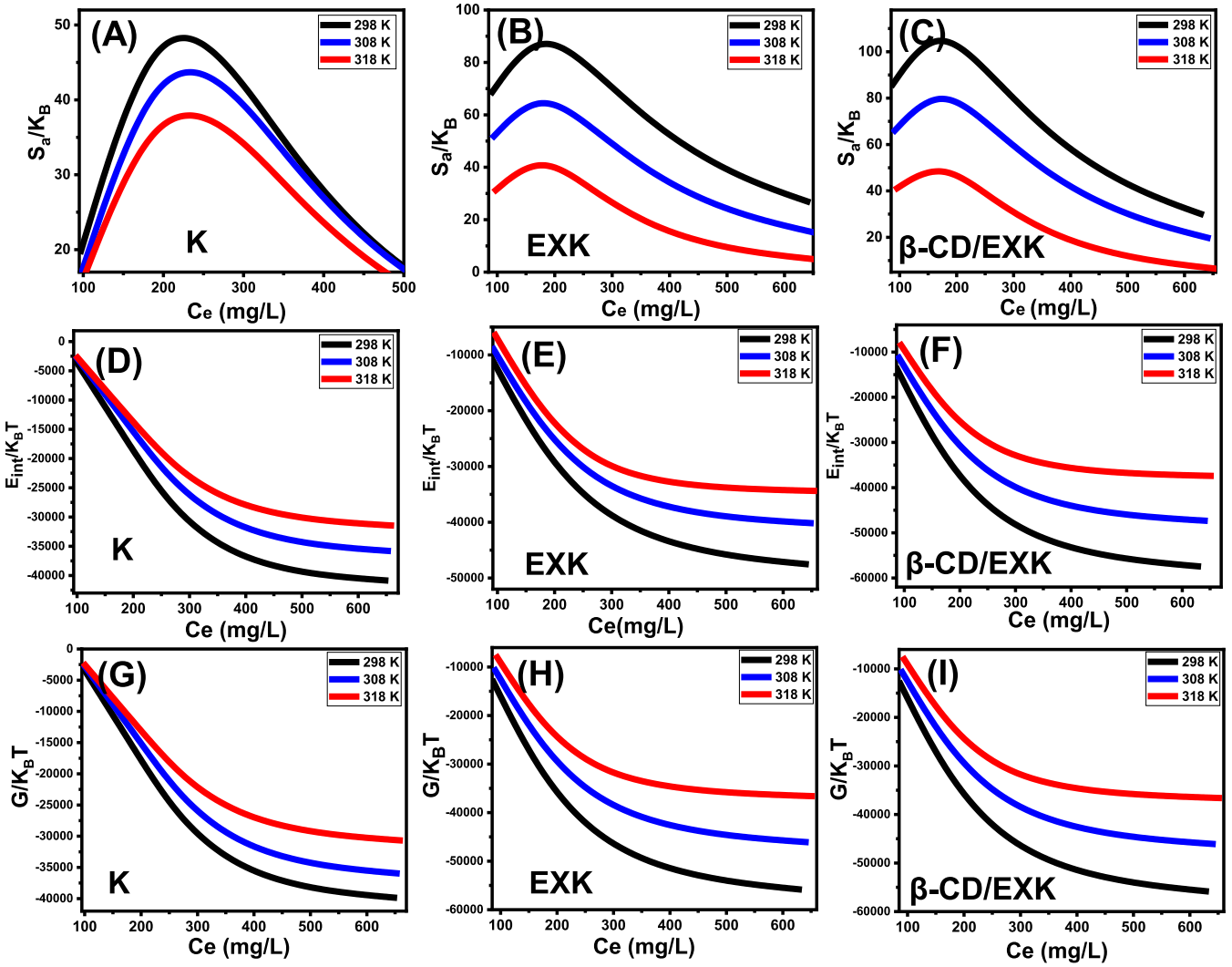

Figure 8. Shows changes in the entropy properties during the uptake of MP[(A) (K), (B) (EXK), and (C) (β-CD/EXK)], changes in the internal energy properties during the uptake of MP [(D) (K), (E) (EXK), and (F) (β-CD/EXK)], and changes in the enthalpy properties during the uptake of MP [(G) (K), (H) (EXK), and (I) (β-CD/EXK)].

https://doi.org/10.1021/acsomega.3c07088
ACS Omega 2023, 8, 48166−48180

to the addressed temperature. Considering the earlier determined values for N_m and n, in addition to the MP concentrations at the half-saturation phases of K, EXK, and β-CD/EXK ($C_{1/2}$), the S_a characteristics were highlighted according to eq 2

$$\frac{S_a}{K_B} = N_m\left\{\ln\left(1+\left(\frac{C}{C_{1/2}}\right)^n\right) - n\left(\frac{C}{C_{1/2}}\right)^n \frac{\ln\left(\frac{C}{C_{1/2}}\right)}{1+\left(\frac{C}{C_{1/2}}\right)^n}\right\} \quad (2)$$

The analyzed curves demonstrate that the magnitudes of the entropy (S_a) values decrease dramatically during the uptake of MP by K, EXK, and β-CD/EXK in the context of very high MP concentrations. This trend demonstrates the remarkable reduction in disorder properties of the surfaces of K, EXK, and β-CD/EXK with rising the analyzed MP concentrations (Figure 8A−C). These entropy properties also support the effective docking of the MP into the existing active sites of K, EXK, and β-CD/EXK, as well as free binding receptors at low concentrations of the pesticide molecules.[56,58] At equilibrium concentrations of 222.61 mg/L (298 K), 220.65 mg/L (308 K), and 218.96 mg/L (313 K), entropy maximal values were observed during the sequestration of MP by K (Figure 8A). The calculated values for the equivalent equilibrium concentrations of maximal entropy utilizing EXK are 165.56 mg/g at 298 K, 160.78 mg/g at 308 K, and 158.34 mg/g at 313 K (Figure 8B). The determined maximum values of entropy for the use of β-CD/EXK as an adsorbent for MP are 153.58 mg/L (298 K), 154.11 mg/L (308 K), and 148.04 mg/L (313 K) (Figure 8C). These equilibrium values fairly match the MP concentrations that are supposed to exist under the half-saturation conditions of K, EXK, and β-CD/EXK. As a consequence, additional MP molecules cannot dock on their free sites. Furthermore, the significant declines in noticed entropy values indicated a significant decline in the number of free sites as well as a noticeable decrease in the freedom and mobility properties of the MP ions.[59]

Internal energy and free enthalpy: The internal energy (E_{int}) that corresponds to the MP uptake operations via K, EXK, and β-CD/EXK as well as free enthalpy (G) aspects and their modifications as a direct consequence of differences in the MP concentrations and acted temperature have been assessed employing the parameters provided by eqs 3 and 4, respectively, depending on the already established N_m, n, and $C_{1/2}$ in the context of the translation partition (Z_v)[55]

$$\frac{E_{int}}{K_B T} = nN_m\left[\left(\frac{\left(\frac{C}{C_{1/2}}\right)^n \ln\left(\frac{C}{Z_v}\right)}{1+\left(\frac{C}{C_{1/2}}\right)^n}\right) - \left(\frac{n\ln\left(\frac{C}{C_{1/2}}\right)\left(\frac{C}{C_{1/2}}\right)^n}{1+\left(\frac{C}{C_{1/2}}\right)^n}\right)\right] \quad (3)$$

$$\frac{G}{K_B T} = nN_m \frac{\ln\left(\frac{C}{Z_v}\right)}{1+\left(\frac{C_{1/2}}{C}\right)^n} \quad (4)$$

The calculated E_{int} values for the MP adsorption processes by K, EXK, and β-CD/EXK are negative, and these findings reveal a drastic decrease once the examined temperature is increased from 298 to 303 K (Figure 8D−F). As a result, K, EXK, and β-CD/EXK's MP uptake processes exhibit more spontaneous in addition to exothermic characteristics. For the predetermined enthalpy values, similar behaviors and characteristics were observed (Figure 8G−I). The G values are negative and possess a reversible correlation with the actual uptake temperature, which denotes a drop in the feasibility features and confirms the spontaneous and exothermic activity of the MP uptake by K, EXK, and β-CD/EXK (Figure 7K,L).

2.2.9. Recyclability. The evaluation of solid-adsorbent materials for commercial as well as practical remediation activities necessitates the consideration of their recycling capacity and reusability characteristics as crucial factors. The β-CD/EXK particulates that were used in the MP adsorption experiments were thoroughly rinsed with distilled water over three cycles. Each cycle took approximately 15 min to complete. Subsequently, the materials were carefully dried for a duration of 10 h at a temperature of 50 °C. The studies were conducted using consistent values for the independent variables, including solid dose (0.2 g/L), time (24 h), volume (100 mL), temperature (298 K), and concentration (200 mg/L). The observed outcomes obtained from the conducted recyclability experiments provide evidence for the notable stability of β-CD/EXK as a prospective adsorbent for MP and MG organic molecules, depending on the examined concentrations. The MP adsorption capacities achieved with β-CD/EXK were as follows: 186.2 mg/g in Run 1, 182.3 mg/g in Run 2, 171.4 mg/g in Run 3, 163.2 mg/g in Run 4, and 151.4 mg/g in Run 5. The observed decline in the adsorption effectiveness of β-CD/EXK with increasing reusability tests can be attributed to a partial reduction in the mass of the dosage as a result of the washing procedures.

2.2.10. Comparison Study. The potential adsorption effectiveness of β-CD/EXK as an adsorbent of MP compounds was evaluated by considering the individual characteristics of its combined parts in their individual phases (β-CD, K, and EXK) (Table 4). The findings of this study indicate that β-CD/EXK exhibits a significantly greater capacity when compared with β-CD, K, and EXK. This observation highlights the importance of the exfoliation and blend techniques in improving the adsorption elimination of MP. These improvements can be attributed to the increased surface area, greater number of active sites for adsorption, and enhanced organic affinities of the K surface. Furthermore, the synthetic β-CD/EXK exhibits better performance compared to the majority of the inorganic and organic adsorbents that have been declared (Table 4). The aforementioned substances comprise activated carbon, cellulose, red soil, chitosan, synthetic zeolite, and clay soil. The previous assertion confirms the efficiency of the obtained β-CD/EXK structure as it serves as an environmentally friendly adsorbent with remarkable adsorption capacity, profitable recyclability, straightforward synthesis methods, cost-effectiveness, abundant precursor materials, and few production byproducts. Hence, the utilization of the β-CD/EXK composite and multifunctional structure has promising efficacy in the practical application of decontaminating dangerous organic contaminants from wastewater.

3. CONCLUSIONS

The adsorption activities of synthetic β-CD hybridized exfoliated kaolinite (β-CD/EXK) as an adsorbent for MP pesticide were assessed considering the synergetic enhancement impact of the exfoliation process (EXK) as well as the polymer integration (β-CD) as compared to raw K. The β-CD/EXK composite revealed remarkable improved uptake behavior (350.6 mg/g) as compared to EXK (291.7 mg/g) and

https://doi.org/10.1021/acsomega.3c07088
ACS Omega 2023, 8, 48166−48180

K (244.7 mg/g). The MP adsorption properties of β-CD/EXK, in addition to the controlling mechanisms, were studied based on the isotherm principals of conventional Langmuir and the significance of advanced monolayer models with one site of energy. The steric parameters validated an observable increase in the total quantities of the existing active sites after the exfoliation step (EXK) (134.4 mg/g) and the integration of the β-CD polymer (162.3 mg/g) as compared to K (75.7 mg/g). This illustrates the significantly greater MP uptake capacities of β-CD/EXK than EXK and K. Furthermore, the detected number of sequestrated MP (up to 3 molecules) demonstrated its uptake via multimolecular mechanisms in vertical arrangements. The evaluated MP uptake energy (<40 kJ/mol) in addition to the thermodynamic functions validates the exothermic, physical, and spontaneous nature of the MP uptake reactions.

4. EXPERIMENTAL WORK

4.1. Materials. The K powder implemented throughout the synthesis processes of individual EXK nanosheets was employed as a purified material and was provided directly from Egypt's Central Metallurgical and Development Institute. Methanol (>99.9%; Sigma-Aldrich; Egypt), dimethyl sulfoxide solution (DMSO) (>99.5%; Sigma-Aldrich; Egypt), and cetyltrimethylammonium bromide powder (CTAB) (>98.8%; Sigma-Aldrich; Egypt) were implemented as the essential chemicals during the sonochemical exfoliation steps. Analytical grade β-CD powder (>85%; MW 1153 g/mol; Sigma-Aldrich; Egypt) and analytical grade ethanol (95%; Sigma-Aldrich; Egypt) were implemented during the synthesis of the composite with the EXK particles. MP (99.9%, Riedel-de Haen; Germany) was applied as the source of the polluted solution during the adsorption studies.

4.2. Synthesis of Exfoliated Kaolinite Nanosheets (EXK). The layered units of K have been exfoliated using a simple sonochemical expansion technique. A ball mill was used to grind K for approximately 6 h, resulting in a fine powder with a size range of 20−100 nm. The pulverized K (15 g) was then extensively homogenized in 50 mL of a slightly dilute DMSO solution [8 (DMSO):1 (distilled water)] throughout a period of 5 h using conventional magnetic stirring equipment. This process must be performed to breakdown the hydrogen bonds that are holding the stratified, layered silicate units together. The resultant (DMSO-intercalated K layers) was then rinsed using methanol for 20 min, and this step was replicated five times to entirely get rid of the embedded DMSO molecules and replace them with the molecules of the used alcohol, yielding an organophilic structure that is referred to as methoxy K (MthK). For 48 h, the developed MthK fine particles were thoroughly homogenized in a formerly produced CTAB solution (20 g CTAB + 50 mL distilled water) utilizing a combination blending system consisting of a magnetic stirrer alongside a high-energy ultrasound radiation source (240 W), triggering K exfoliation or splitting into individual and single nanosheets (EXK). Afterward, the newly produced EXK nanoparticles were carefully rinsed using distilled water and then dried gently at 65 °C for 12 h.

4.3. Synthesis of β-CD/EXK. The combination of EXK nanostructures with the β-CD has been completed in accordance with the approach outlined by Altoom et al.[40] The certain weight of β-CD (1 g) was dispersed and homogenized in about 80 mL of pure ethanol over a period of 3 h employing a magnetic stirring device (1000 rpm), resulting in a slurry-like fluid. In an interconnected experiment, 2 g of already developed EXK fractions have been added to 100 mL of distilled water and mixed for 60 min while rotating at 1000 rpm and under ultrasound power of 240 W. The resulting EXK slurry and β-CD solution were then combined, and the mixing process was carried out by a magnetic stirrer (at 1000 rpm) for a period of 24 h. The remaining solution was subsequently homogenized another time using an ultrasound generator (240 W) for an additional 24 h. The hybrid particulates were then gently filtered from the mixture using Whatman filter paper (40 μm). The resultant β-CD/EXK product had been rinsed using distilled water to neutralize its surface and finally dried for 12 h at 60 °C prior to being employed in the following tests.

4.4. Analytical Techniques. The degree of crystallization and the crystalline phases have been identified by utilizing a PANalytical-Empyrean X-ray diffractometer. The utilized apparatus is equipped with Cu-Kα radiation, and the analyses were performed within the angular range of 5−70°. The scanning rate employed was 5°/min, while a constant voltage of 40 kV was maintained during the procedure. The chemical structures of EXK and β-CD/EXK, as well as the produced transitional materials, were distinguished by using a FT-IR spectrometer (FTIR8400S; Shimadzu). This measurement's detecting range of frequencies was 400 to 4000 cm^{-1}. The investigation was performed following the adjustment of the setup conditions at a resolution of 4 cm^{-1} and a total of 37 scans. The SEM photos (Gemini, Zeiss Ultra 55) were gathered immediately after the fabricated clay structures had been topped with a thin sheet of gold using various accelerating voltages ranging from 5 to 30 kV. A transmission electron microscope (JEOL-JEM2100) was utilized for gathering the HRTEM images, which were subsequently employed to evaluate the internal characteristics of both EXK and β-CD/EXK at an acceleration voltage of around 200 kV. Using a surface area analyzer (Beckman Coulter SA3100), both the porosity and surface area of EXK and β-CD/EXK were evaluated, depending on their correlated N_2 adsorption and desorption isotherms.

4.5. Adsorption Studies. The adsorption procedures of MP using K, EXK, and β-CD/EXK have been performed as a batch study employing frequently applied experimental variables such as pH (2 to 9), adsorption duration (30 to 840 min), and MP concentration (100 to 700 mg/L) together with regular variation in the experimental temperature from 298 to 313 K. Additionally, the other main experimental key parameters were selected at certain and adjusted values throughout the study [volume: 100 mL and solid dosage: 0.2 g/L]. The experimental approach was assessed in triplicate by using the mean values of all determined concentrations and the estimated calculations and findings. After the equilibrium period for all of the adsorption examinations, the solid particulates of K, EXK, and β-CD/EXK were separated from the implemented MP solutions using Whatman filter paper. The rest of the concentrations of MP have been determined using a HPLC system (Merck/Hitachi) that consisted of an injection valve (Rheodyne 7725i), a pump (L-7100), a detector (L-7400), a Luna column (150 mm × 4.6 mm), and a sample loop (20 mL). The stationary phase of the HPLC column (Phenomenex, Torrance, USA) is made of PFP having a thickness of 5 mm. The MP adsorption capacities (Q_e) of K, EXK, and β-CD/EXK in mg/g were calculated using eq 5, considering also the treated MP volume (V), the dosages of K,

https://doi.org/10.1021/acsomega.3c07088
ACS Omega 2023, 8, 48166−48180

EXK, and β-CD/EXK (m), the initial MP concentration (C_o), and the rest MP concentration (C_e)

$$Q_{e(mg/g)} = \frac{(C_o - C_e)V}{m} \quad (5)$$

4.6. Theoretical Traditional and Advanced Equilibrium Studies. The adsorption experiments were theoretically modeled using classical kinetic, classic isotherm, and advanced isotherm modeling based on statistical physics hypotheses (Table S1). The kinetic and classic equilibrium modeling were conducted using nonlinear fitting procedures utilizing the theoretical formulas of these models and the resultant values of R^2 (eq 5a) in addition to χ^2 (eq 6). The fitting levels of the adsorption processes with the evaluated advanced equilibrium models were determined using R^2 and the root-mean-square error (RMSE) (eq 7). The m', p, Qi_{cal}, and Qi_{exp} symbols represent the obtained experimental results, investigated factors, assumed MP adsorption, and validated adsorption capacity, respectively

$$R^2 = 1 - \frac{\sum (q_{e,exp} - q_{e,cal})^2}{\sum (q_{e,exp} - q_{e,mean})^2} \quad (5a)$$

$$\chi^2 = \frac{(q_{e,exp} - q_{e,cal})^2}{q_{e,cal}} \quad (6)$$

$$RMSE = \sqrt{\frac{\sum_{i=1}^{m} (Qi_{cal} - Qi_{exp})^2}{m' - p}} \quad (7)$$

■ ASSOCIATED CONTENT

Supporting Information

The Supporting Information is available free of charge at https://pubs.acs.org/doi/10.1021/acsomega.3c07088.

Representative equations of the kinetic and isotherm models and SEM image of the synthetic β-CD/EXK composite (PDF)

■ AUTHOR INFORMATION

Corresponding Authors

Wail Al Zoubi − *Materials Electrochemistry Laboratory, School of Materials Science and Engineering, Yeungnam University, Gyeongsan 38541, Republic of Korea;* orcid.org/0000-0003-4213-8481; Email: wailalzoubi@ynu.ac.kr

Mostafa R. Abukhadra − *Geology Department, Faculty of Science, Beni-Suef University, Beni Suef City 62511, Egypt; Materials Technologies and Their Applications Lab, Faculty of Science, Beni-Suef University, Beni Suef City 62511, Egypt;* orcid.org/0000-0001-5404-7996; Phone: +2001288447189; Email: Abukhadra89@Science.bsu.edu.eg

Authors

Nourhan Nasser − *Geology Department, Faculty of Science, Beni-Suef University, Beni Suef City 62511, Egypt; Materials Technologies and Their Applications Lab, Faculty of Science, Beni-Suef University, Beni Suef City 62511, Egypt*

Ahmed Rady − *Department of Zology, College of Science, King Saud University, Riyadh 11451, Saudi Arabia*

Ahmed A. Allam − *Zoology Department, Faculty of Science, Beni-Suef University, Beni-Suef 62511, Egypt*

Complete contact information is available at: https://pubs.acs.org/10.1021/acsomega.3c07088

Author Contributions

This article was written through the contributions of all authors. All authors have given their approval to the final version of the manuscript.

Notes

The authors declare no competing financial interest.

■ ACKNOWLEDGMENTS

The authors extend their appreciation to King Saud University for funding this work through Researchers Supporting Project no. (RSP2023R691), King Saud University, Riyadh, Saudi Arabia.

■ REFERENCES

(1) Benisha, R.; Amalanathan, M.; Aravind, M.; Mary, M. S. M.; Ahmad, A.; Tabassum, S.; Al-Qahtani, W. H.; Ahmad, I. Catharanthus Roseus Leaf Extract Mediated Ag-MgO Nanocatalyst for Photocatalytic Degradation of Congo Red Dye and Their Antibacterial Activity. *J. Mol. Struct.* **2022**, *1262*, 133005.

(2) Abdel Salam, M.; Mokhtar, M.; Albukhari, S. M.; Baamer, D. F.; Palmisano, L.; Jaremko, M.; Abukhadra, M. R. Synthesis and Characterization of Green ZnO@polynaniline/Bentonite Tripartite Structure (G.Zn@PN/BE) as Adsorbent for As (V) Ions: Integration, Steric, and Energetic Properties. *Polymers* **2022**, *14* (12), 2329.

(3) Jiang, Y.; Abukhadra, M. R.; Refay, N. M.; Sharaf, M. F.; El-Meligy, M. A.; Awwad, E. M. Synthesis of Chitosan/MCM-48 and β-Cyclodextrin/MCM-48 Composites as Bio-Adsorbents for Environmental Removal of Cd2+ Ions; Kinetic and Equilibrium Studies. *React. Funct. Polym.* **2020**, *154*, 104675.

(4) Kaur, J.; Singh, P. K. Enzyme-Based Optical Biosensors for Organophosphate Class of Pesticide Detection. *Phys. Chem. Chem. Phys.* **2020**, *22* (27), 15105−15119.

(5) Rani, M.; Shanker, U. Degradation of Traditional and New Emerging Pesticides in Water by Nanomaterials: Recent Trends and Future Recommendations. *Int. J. Environ. Sci. Technol.* **2018**, *15* (6), 1347−1380.

(6) Mohamed, A. S.; Abukkhadra, M. R.; Abdallah, E. A.; El-Sherbeeny, A. M.; Mahmoud, R. K. The Photocatalytic Performance of Silica Fume Based Co3O4/MCM-41 Green Nanocomposite for Instantaneous Degradation of Omethoate Pesticide under Visible Light. *J. Photochem. Photobiol., A* **2020**, *392*, 112434.

(7) Abukhadra, M. R.; AlHammadi, A.; El-Sherbeeny, A. M.; Salam, M. A.; El-Meligy, M. A.; Awwad, E. M.; Luqman, M. Enhancing the Removal of Organic and Inorganic Selenium Ions Using an Exfoliated Kaolinite/Cellulose Fibres Nanocomposite. *Carbohydr. Polym.* **2021**, *252*, 117163.

(8) Tan, D.; Yuan, P.; Dong, F.; He, H.; Sun, S.; Liu, Z. Selective Loading of 5-Fluorouracil in the Interlayer Space of Methoxy-Modified Kaolinite for Controlled Release. *Appl. Clay Sci.* **2018**, *159*, 102−106.

(9) Yang, L.; Hai, C.; Zhang, H.; Feng, C.; Luo, M.; Zhou, P.; Leng, J.; Tian, X.; Zhao, C.; Lai, B. Insights into the Role of Oxidation and Adsorption for Degradation of Methyl Parathion by Ferrate (VI). *J. Environ. Chem. Eng.* **2023**, *11* (3), 110171.

(10) Ilager, D.; Shetti, N. P.; Foucaud, Y.; Badawi, M.; Aminabhavi, T. M. Graphene/g-Carbon Nitride (GO/g-C3N4) Nanohybrids as a Sensor Material for the Detection of Methyl Parathion and Carbendazim. *Chemosphere* **2022**, *292*, 133450.

(11) Mohammadi, P.; Sheibani, H. Evaluation, of the Bimetallic Photocatalytic Performance of Resin-Au-Pd Nanocomposite for

Degradation of Parathion Pesticide under Visible Light. *Polyhedron* **2019**, *170*, 132−137.
(12) Abukhadra, M. R.; Saad, I.; Othman, S. I.; Katowah, D. F.; Ajarem, J. S.; Alqarni, S. A.; Allam, A. A.; Al Zoubi, W.; Gun Ko, Y. Characterization of Fe0@Chitosan/Cellulose Structure as Effective Green Adsorbent for Methyl Parathion, Malachite Green, and Levofloxacin Removal: Experimental and Theoretical Studies. *J. Mol. Liq.* **2022**, *368*, 120730.
(13) Salam, M. A.; AbuKhadra, M. R.; Mohamed, A. S. Effective Oxidation of Methyl Parathion Pesticide in Water over Recycled Glass Based-MCM-41 Decorated by Green Co3O4 Nanoparticles. *Environ. Pollut.* **2020**, *259*, 113874.
(14) Manga Raju, I.; T, S. R.; K.V, D. L.; M, R. C.; J, S. P.; G, D. Poly 3-Thenoic Acid Sensitized, Copper Doped Anatase/Brookite TiO2 Nanohybrids for Enhanced Photocatalytic Degradation of an Organophosphorus Pesticide. *J. Environ. Chem. Eng.* **2019**, *7* (4), 103211.
(15) Ramya, E.; Thirumurugan, A.; Rapheal, V. S.; Anand, K. CuO@SiO2 Nanoparticles Assisted Photocatalytic Degradation of 4-Nitrophenol and Their Antimicrobial Activity Studies. *Environ. Nanotechnol. Monit. Manag.* **2019**, *12*, 100240.
(16) Debnath, D.; Gupta, A. K.; Ghosal, P. S. Recent Advances in the Development of Tailored Functional Materials for the Treatment of Pesticides in Aqueous Media: A Review. *J. Ind. Eng. Chem.* **2019**, *70*, 51−69.
(17) Yang, X.; Wang, J.; El-Sherbeeny, A. M.; AlHammadi, A. A.; Park, W.-H.; Abukhadra, M. R. Insight into the Adsorption and Oxidation Activity of a ZnO/Piezoelectric Quartz Core-Shell for Enhanced Decontamination of Ibuprofen: Steric, Energetic, and Oxidation Studies. *Chem. Eng. J.* **2022**, *431*, 134312.
(18) Mostafa, M.; Bin Jumah, M. N.; Othman, S. I.; Alruhaimi, R. S.; Salama, Y. F.; Allam, A. A.; Abukhadra, M. R. Effective Removal of Different Species of Organophosphorus Pesticides (Acephate, Omthosate, and Methyl Parathion) Using Chitosan/Zeolite-A as Multifunctional Adsorbent. *Environ. Technol. Innovat.* **2021**, *24*, 101875.
(19) Park, J.-E.; Lee, M.-Y.; Kim, S.-H.; Song, S.-M.; Park, B.-K.; Seo, S.-J.; Song, J.-Y.; Hur, M.-J. A Survey on the Residual Pesticides on Agricultural Products on the Markets in Incheon from 2016 to 2018. *Korean Journal of Environmental Agriculture* **2019**, *38* (3), 205−212.
(20) Sayed, I. R.; Farhan, A. M.; AlHammadi, A. A.; El-Sayed, M. I.; Abd El-Gaied, I. M.; El-Sherbeeny, A. M.; Al Zoubi, W.; Ko, Y. G.; Abukhadra, M. R. Synthesis of Novel Nanoporous Zinc Phosphate/Hydroxyapatite Nano-Rods (ZPh/HPANRs) Core/Shell for Enhanced Adsorption of Ni2+ and Co2+ Ions: Characterization and Application. *J. Mol. Liq.* **2022**, *360*, 119527.
(21) Abukhadra, M. R.; Saad, I.; Al Othman, S. I.; Alfassam, H. E.; Allam, A. A. Insight into the Synergetic, Steric and Energetic Properties of Zeolitization and Cellulose Fiber Functionalization of Diatomite during the Adsorption of Cd(Ii): Advanced Equilibrium Studies. *RSC Adv.* **2023**, *13* (34), 23601−23618.
(22) Abukhadra, M. R.; Mostafa, M.; El-Sherbeeny, A. M.; El-Meligy, M. A.; Nadeem, A. Instantaneous Adsorption of Synthetic Dyes from an Aqueous Environment Using Kaolinite Nanotubes: Equilibrium and Thermodynamic Studies. *ACS Omega* **2021**, *6* (1), 845−856.
(23) Çiftçi, H. Removal of Methylene Blue from Water by Ultrasound-Assisted Adsorption Using Low-Cost Bentonites. *Chem. Phys. Lett.* **2022**, *802*, 139758.
(24) Tian, L.; Abukhadra, M. R.; Mohamed, A. S.; Nadeem, A.; Ahmad, S. F.; Ibrahim, K. E. Insight into the Loading and Release Properties of an Exfoliated Kaolinite/Cellulose Fiber (EXK/CF) Composite as a Carrier for Oxaliplatin Drug: Cytotoxicity and Release Kinetics. *ACS Omega* **2020**, *5* (30), 19165−19173.
(25) Alqahtani, M. D.; Nasser, N.; Bin Jumah, M. N.; AlZahrani, S. A.; Allam, A. A.; Abukhadra, M. R.; Bellucci, S. Insight into the Morphological Properties of Nano-Kaolinite (Nanoscrolls and Nanosheets) on Its Qualification as Delivery Structure of Oxaliplatin: Loading, Release, and Kinetic Studies. *Molecules* **2023**, *28* (13), 5158.
(26) Shaban, M.; Sayed, M. I.; Shahien, M. G.; Abukhadra, M. R.; Ahmed, Z. M. Adsorption Behavior of Inorganic- and Organic-Modified Kaolinite for Congo Red Dye from Water, Kinetic Modeling, and Equilibrium Studies. *J. Sol-Gel Sci. Technol.* **2018**, *87* (2), 427−441.
(27) Carretero, M. I.; Pozo, M. Clay and Non-Clay Minerals in the Pharmaceutical and Cosmetic Industries Part II. Active Ingredients. *Appl. Clay Sci.* **2010**, *47* (3−4), 171−181.
(28) Abukhadra, M. R.; Allah, A. F. Synthesis and Characterization of Kaolinite Nanotubes (KNTs) as a Novel Carrier for 5-Fluorouracil of High Encapsulation Properties and Controlled Release. *Inorg. Chem. Commun.* **2019**, *103*, 30−36.
(29) Alqahtani, M. D.; Nasser, N.; Bin Jumah, M. N.; AlZahrani, S. A.; Allam, A. A.; Abukhadra, M. R.; Bellucci, S. Synthesis and Characterization of β-Cyclodextrin-Hybridized Exfoliated Kaolinite Single Nanosheets as Potential Carriers of Oxaliplatin with Enhanced Loading, Release, and Cytotoxic Properties. *Materials* **2023**, *16* (14), 4958.
(30) Abukhadra, M. R.; El-Sherbeeny, A. M.; El-Meligy, M. A.; Luqman, M. Insight into Carbohydrate Polymers (Chitosan and 2-Hydroxyethyl Methacrylate/Methyl Methacrylate) Intercalated Bentonite-Based Nanocomposites as Multifunctional and Environmental Adsorbents for Methyl Parathion Pesticide. *Int. J. Biol. Macromol.* **2021**, *167*, 335−344.
(31) Ashraf, M.-T.; AlHammadi, A. A.; El-Sherbeeny, A. M.; Alhammadi, S.; Al Zoubi, W.; Ko, Y. G.; Abukhadra, M. R. Synthesis of Cellulose Fibers/Zeolite-A Nanocomposite as an Environmental Adsorbent for Organic and Inorganic Selenium Ions; Characterization and Advanced Equilibrium Studies. *J. Mol. Liq.* **2022**, *360*, 119573.
(32) Faraji Dizaji, B.; Hasani Azerbaijan, M.; Sheisi, N.; Goleij, P.; Mirmajidi, T.; Chogan, F.; Irani, M.; Sharafian, F. Synthesis of PLGA/Chitosan/Zeolites and PLGA/Chitosan/Metal Organic Frameworks Nanofibers for Targeted Delivery of Paclitaxel toward Prostate Cancer Cells Death. *Int. J. Biol. Macromol.* **2020**, *164*, 1461−1474.
(33) Servatan, M.; Zarrintaj, P.; Mahmodi, G.; Kim, S.-J.; Ganjali, M. R.; Saeb, M. R.; Mozafari, M. Zeolites in Drug Delivery: Progress, Challenges and Opportunities. *Drug Discovery Today* **2020**, *25* (4), 642−656.
(34) El-Zeiny, H. M.; Abukhadra, M. R.; Sayed, O. M.; Osman, A. H. M.; Ahmed, S. A. Insight into Novel β-Cyclodextrin-Grafted-Poly (N-Vinylcaprolactam) Nanogel Structures as Advanced Carriers for 5-Fluorouracil: Equilibrium Behavior and Pharmacokinetic Modeling. *Colloids Surf., A* **2020**, *586*, 124197.
(35) Sadjadi, S.; Koohestani, F. Composite of β-Cyclodextrin and Bentonite Clay: A Promising Support for Pd Immobilization and Developing a Catalyst for Hydrogenation of Nitroarenes under Mild Reaction Condition. *J. Phys. Chem. Solids* **2021**, *151*, 109894.
(36) Krawczyk, K.; Silvestri, D.; Nguyen, N. H. A.; Ševců, A.; Łukowiec, D.; Padil, V. V. T.; Řezanka, M.; Černík, M.; Dionysiou, D. D.; Wacławek, S. Enhanced Degradation of Sulfamethoxazole by a Modified Nano Zero-Valent Iron with a β-Cyclodextrin Polymer: Mechanism and Toxicity Evaluation. *Sci. Total Environ.* **2022**, *817*, 152888.
(37) El-Sherbeeny, A. M.; Ibrahim, S. M.; AlHammadi, A. A.; Soliman, A. T. A.; Shim, J.-J.; Abukhadra, M. R. Effective Retention of Radioactive Cs^{+} and Ba^{2+} Ions Using β-Cyclodextrin Functionalized Diatomite (β-CD/D) as Environmental Adsorbent; Characterization, Application, and Safety. *Surface. Interfac.* **2021**, *26*, 101434.
(38) Bandura, L.; Białoszewska, M.; Malinowski, S.; Franus, W. Adsorptive Performance of Fly Ash-Derived Zeolite Modified by β-Cyclodextrin for Ibuprofen, Bisphenol A and Caffeine Removal from Aqueous Solutions - Equilibrium and Kinetic Study. *Appl. Surf. Sci.* **2021**, *562*, 150160.
(39) Bin Jumah, M. N.; Eid, M. H.; Al-Huqail, A. A.; Mohammad, M. A.; Bin-Murdhi, N. S.; Abu-Taweel, G. M.; Altoom, N.; Allam, A. A.; AbuKhadra, M. R. Enhanced Remediation of As (V) and Hg (II) Ions from Aqueous Environments Using β-Cyclodextrin/MCM-48

https://doi.org/10.1021/acsomega.3c07088
ACS Omega 2023, 8, 48166−48180

Composite: Batch and Column Studies. *J. Water Proc. Eng.* **2021**, *42*, 102118.
(40) Altoom, N.; Ibrahim, S. M.; Othman, S. I.; Allam, A. A.; Alqhtani, H. A.; Al-Otaibi, F. S.; Abukhadra, M. R. Characterization of β-Cyclodextrin/Phillipsite (β-CD/Ph) Composite as a Potential Carrier for Oxaliplatin as Therapy for Colorectal Cancer; Loading, Release, and Cytotoxicity. *Colloids Surf., A* **2022**, *648*, 129144.
(41) Adly, E. R.; Shaban, M. S.; El-Sherbeeny, A. M.; Al Zoubi, W.; Abukhadra, M. R. Enhanced Congo Red Adsorption and Photo-Fenton Oxidation over an Iron-Impeded Geopolymer from Ferruginous Kaolinite: Steric, Energetic, Oxidation, and Synergetic Studies. *ACS Omega* **2022**, *7* (35), 31218−31232.
(42) Shawky, A.; El-Sheikh, S. M.; Rashed, M. N.; Abdo, S. M.; El-Dosoqy, T. I. Exfoliated Kaolinite Nanolayers as an Alternative Photocatalyst with Superb Activity. *J. Environ. Chem. Eng.* **2019**, *7* (3), 103174.
(43) Vivas, E. L.; Cho, K. Efficient Adsorptive Removal of Cobalt(II) Ions from Water by Dicalcium Phosphate Dihydrate. *J. Environ. Manage.* **2021**, *283*, 111990.
(44) Salam, M. A.; Abukhadra, M. R.; Mostafa, M. Effective Decontamination of As(V), Hg(II), and U(VI) Toxic Ions from Water Using Novel Muscovite/Zeolite Aluminosilicate Composite: Adsorption Behavior and Mechanism. *Environ. Sci. Pollut. Res.* **2020**, *27* (12), 13247−13260.
(45) Othman, S. I.; Alqhtani, H. A.; Allam, A. A.; Rabie, A. M.; Abdelrahman, A. A.; Salem, H. M.; Abukhadra, M. R. Insight into the Adsorption Properties of a β-Cyclodextrin/Phillipsite Organophilic Composite for Effective Removal of Toxic Organophosphorus Pesticides: Kinetic and Advanced Equilibrium Studies. *New J. Chem.* **2022**, *46* (40), 19419−19431.
(46) El Qada, E. Kinetic Behavior of the Adsorption of Malachite Green UsingJordanian Diatomite as Adsorbent. *JORDANIAN JOURNAL OF ENGINEERING AND CHEMICAL INDUSTRIES (JJECI)* **2020**, *3* (1), 1−10.
(47) Lin, X.; Xie, Y.; Lu, H.; Xin, Y.; Altaf, R.; Zhu, S.; Liu, D. Facile Preparation of Dual La-Zr Modified Magnetite Adsorbents for Efficient and Selective Phosphorus Recovery. *Chem. Eng. J.* **2021**, *413*, 127530.
(48) Albukhari, S. M.; Salam, M. A.; Abukhadra, M. R. Effective Retention of Inorganic Selenium Ions (Se (VI) and Se (IV)) Using Novel Sodalite Structures from Muscovite; Characterization and Mechanism. *J. Taiwan Inst. Chem. Eng.* **2021**, *120*, 116−126.
(49) Sherlala, A. I. A.; Raman, A. A. A.; Bello, M. M.; Buthiyappan, A. Adsorption of Arsenic Using Chitosan Magnetic Graphene Oxide Nanocomposite. *J. Environ. Manage.* **2019**, *246*, 547−556.
(50) Huang, Y.; Zeng, X.; Guo, L.; Lan, J.; Zhang, L.; Cao, D. Heavy Metal Ion Removal of Wastewater by Zeolite-Imidazolate Frameworks. *Sep. Purif. Technol.* **2018**, *194*, 462−469.
(51) Jasper, E. E.; Ajibola, V. O.; Onwuka, J. C. Nonlinear Regression Analysis of the Sorption of Crystal Violet and Methylene Blue from Aqueous Solutions onto an Agro-Waste Derived Activated Carbon. *Appl. Water Sci.* **2020**, *10* (6), 132.
(52) Abukhadra, M. R.; Dardir, F. M.; Shaban, M.; Ahmed, E. A.; Soliman, M. F. Superior Removal of Co2+, Cu2+ and Zn2+ Contaminants from Water Utilizing Spongy Ni/Fe Carbonate-Fluorapatite; Preparation, Application and Mechanism. *Ecotoxicol. Environ. Saf.* **2018**, *157*, 358−368.
(53) Faisal M, L. F. M. Batch Sorption of Copper (II) Ions from Simulated Aqueous Solution by Banana Peel. *Al-Khwarizmi Engineering Journal* **2017**, *12* (4), 117−125.
(54) Mobarak, M.; Ali, R. A. M.; Seliem, M. K. Chitosan/Activated Coal Composite as an Effective Adsorbent for Mn(VII): Modeling and Interpretation of Physicochemical Parameters. *Int. J. Biol. Macromol.* **2021**, *186*, 750−758.
(55) Dhaouadi, F.; Sellaoui, L.; Reynel-Ávila, H. E.; Landín-Sandoval, V.; Mendoza-Castillo, D. I.; Jaime-Leal, J. E.; Lima, E. C.; Bonilla-Petriciolet, A.; Lamine, A. B. Adsorption Mechanism of Zn2+, Ni2+, Cd2+, and Cu2+ Ions by Carbon-Based Adsorbents: Interpretation of the Adsorption Isotherms via Physical Modelling. *Environ. Sci. Pollut. Res.* **2021**, *28* (24), 30943−30954.
(56) Sellaoui, L.; Ali, J.; Badawi, M.; Bonilla-Petriciolet, A.; Chen, Z. Understanding the Adsorption Mechanism of Ag+ and Hg2+ on Functionalized Layered Double Hydroxide via Statistical Physics Modeling. *Appl. Clay Sci.* **2020**, *198*, 105828.
(57) Ali, R. A. M.; Mobarak, M.; Badawy, A. M.; Lima, E. C.; Seliem, M. K.; Ramadan, H. S. New Insights into the Surface Oxidation Role in Enhancing Congo Red Dye Uptake by Egyptian Ilmenite Ore: Experiments and Physicochemical Interpretations. *Surface. Interfac.* **2021**, *26*, 101316.
(58) Dhaouadi, F.; Sellaoui, L.; Badawi, M.; Reynel-Ávila, H. E.; Mendoza-Castillo, D. I.; Jaime-Leal, J. E.; Bonilla-Petriciolet, A.; Lamine, A. B. Statistical Physics Interpretation of the Adsorption Mechanism of Pb2+, Cd2+ and Ni2+ on Chicken Feathers. *J. Mol. Liq.* **2020**, *319*, 114168.
(59) Sellaoui, L.; Guedidi, H.; SarraWjihi, S.; Reinert, L.; Knani, S.; Duclaux, L.; Ben Lamine, A. Experimental and Theoretical Studies of Adsorption of Ibuprofen on Raw and Two Chemically Modified Activated Carbons: New Physicochemical Interpretations. *RSC Adv.* **2016**, *6* (15), 12363−12373.
(60) Gupta, V. K.; Gupta, B.; Rastogi, A.; Agarwal, S.; Nayak, A. Pesticides Removal from Waste Water by Activated Carbon Prepared from Waste Rubber Tire. *Water Res.* **2011**, *45* (13), 4047−4055.
(61) Abukhadra, M. R.; Shemy, M. H.; Khim, J. S.; Ajarem, J. S.; Rabie, A. M.; Abdelrahman, A. A.; Allam, A. A.; Salem, H. M.; Shaban, M. S. Insight into the Adsorption Properties of β-Cyclodextrin/Zeolite-A Structure for Effective Removal of Cd2+, PO43-and Methyl Parathion; Kinetics and Advanced Equilibrium Studies. *J. Inorg. Organomet. Polym. Mater.* **2022**, *32* (12), 4664−4678.
(62) N'diaye, A. D.; Boudokhane, C.; Elkory, M. B.; Kankou, M.; Dhaouadi, H. Methyl Parathion Pesticide Removal from Aqueous Solution Using Senegal River Typha Australis. *Water Supply* **2018**, *18* (5), 1545−1553.
(63) Rama Krishna, K.; Philip, L. Adsorption and Desorption Characteristics of Lindane, Carbofuran and Methyl Parathion on Various Indian Soils. *J. Hazard. Mater.* **2008**, *160* (2−3), 559−567.
(64) Abukhadra, M. R.; Saad, I.; Othman, S. I.; Katowah, D. F.; Ajarem, J. S.; Alqarni, S. A.; Allam, A. A.; Al Zoubi, W.; Gun Ko, Y. Characterization of Fe0@Chitosan/Cellulose Structure as Effective Green Adsorbent for Methyl Parathion, Malachite Green, and Levofloxacin Removal: Experimental and Theoretical Studies. *J. Mol. Liq.* **2022**, *368*, 120730.

https://doi.org/10.1021/acsomega.3c07088
ACS Omega 2023, 8, 48166−48180